# Supporting Information

**A Dual-Heterostructure Enables the Stabilization of 1T-rich $MoSe_2$ for Enhanced Sodium Ion Storage**

Yunfeng Chao,[a] Shenghui Jia,[a] Jinzhao Li,[a] Guohui Chen,[a] Lu Liu,[a] Fei Tang,[a] Jianhua Zhu,*[a] Caiyun Wang*[b] and Xinwei Cui[a]

[a]*Henan Institute of Advanced Technology, Zhengzhou University, Zhengzhou 450052, China.*
[b]*Intelligent Polymer Research Institute, Faculty of Engineering and Information Sciences, Innovation Campus, University of Wollongong, North Wollongong, NSW 2500, Australia.*
* Corresponding Authors: jianhuazhu@zzu.edu.cn; caiyun@uow.edu.au

# Table of Contents

# Experimental Section

**Chemicals and materials**

Copper (II) nitrate trihydrate (98.0%), sodium molybdate dihydrate (99%), selenium powders (99.999%), hydrazine hydrate solution (98%), N-methyl-2-pyrrolidone (99%) and metal sodium (99.7%) were purchased from Shanghai Aladdin Biochemical Technology Co., Ltd (China). Polyvinylidene fluoride (PVDF, HSV900) was purchased from Arkema Kynar. Super P was bought from TIMCAL. Glass fiber separators of GF/D type were obtained from Whatman. Electrolyte was purchased from Dodochem Co., Ltd (China). All the chemicals and materials were used as received without any purification or treatment. The deionized water used in all experiments was obtained by ion exchange and filtration.

**Fabrication of G-$Cu_2Se$@$MoSe_2$**

G-$Cu_2Se$@$MoSe_2$ was synthesized through a facial one-pot hydrothermal process. GO was prepared through a modified Hummer's method.[1] The obtained GO dispersion was diluted to 1.6 mg $mL^{-1}$ for use. Then 2 mmol of $Cu(NO_3)_2 \cdot 3H_2O$ and 2 mmol of $Na_2MoO_4 \cdot 2H_2O$ were added into 50 ml of GO dispersion in sequence. After stirring for 30 mins, a solution containing 8 mmol of selenium powders and 12 mL of hydrazine hydrate solution were added. The resulting mixture was transferred into a 100 mL Teflon-lined stainless-steel autoclave and maintained at 180°C in an oven for 24 hours. Then the precipitates were collected by centrifugation, rinsed with deionized water and ethanol, and then vacuum dried at 60°C for 12 hours. The product was placed in a ceramic boat and calcined in a tube furnace at 500°C under an Ar flow at a heating rate of 2 ℃ min-1 for 2 hours to remove the impurities. The control samples of $Cu_2Se$/$MoSe_2$ and G-$MoSe_2$ were prepared following the same procedure by substituting the GO dispersion with deionized water and without the addition of $Cu(NO_3)_2 \cdot 3H_2O$, respectively.

**Material Characterizations**

SEM images were collected using a Zeiss-G300 to examine the morphology and microstructures of samples. TEM and EDS mapping images were obtained from a JEOL-2100F. X-ray diffraction (XRD, Rigaku UlittimalV, Cu Kα radiation) patterns was conducted to analyze the crystal structures. Raman spectra was recorded by a confocal Raman spectrometer (LabRAM Soleil Nano, Horiba). X-ray photoelectron spectroscopy (XPS) was performed using a ESCALAB 250Xianalyzer (ThermoFisher) to characterize the chemical states. $N_2$ adsorption-desorption tests and Braeuer-Emmett-Teller (BET) data were acquired with a Micromeritics ASAP2420 instrument at 77K.

**Electrochemical Measurements**

The electrochemical performance of the composites was evaluated by assembling the

G-$Cu_2Se$@$MoSe_2$ anodes CR2032 coin cells in an argon-filled glovebox (Vigor, LG2400/750TS) with metallic sodium as the counter electrodes and glass-fiber membranes as separators. The working electrodes were prepared by pasting the uniform slurry composed of active material, Super P and polyvinylidene fluoride (PVDF) at a weight ratio of 8:1:1 in N-methyl pyrrolidone (NMP) onto a copper foil, and dried in a vacuum oven at 60 °C for 24 h. The average mass loading of active material in the electrode was in the range of ~1.1 mg $cm^{-2}$. The electrolyte was 1.0 M $NaPF_6$ in dimethyl ether (DoDoChem, China). Galvanostatic charge/discharge and galvanostatic intermittent titration technique (GITT) profiles were measured by a Neware battery testing system (CT4008, China) in the potential window of 0.1-2.5 V (vs Na/$Na^+$). Biologic working station (VSP-3E, France) was selected to collect the cyclic voltammograms (CV) and impendence data under a condition of 0.1 - 2.5 V and $10^5$ - 0.01 Hz, respectively. For the full cell, $Na_3V_2(PO_4)_3$ (NVP) electrodes with a mass loading of ~4.5 mg $cm^{-2}$ was served as the cathodes. The of G-$Cu_2Se$@$MoSe_2$//NVP full cells with a N/P ratio of 0.9 were performed over the voltage range of 0.5-3.5V to collect their electrochemical performance.

**DFT Calculations**

Vienna Ab-inito Simulation Package (VASP) was used to implement density functional theories (DFT) calculations.[2,3] The Perdew-Burke-Ernzerhof (PBE) functional within the generalized gradient approximation (GGA) method was applied to characterize the exchange-correlation effects.[4,5] The projected augmented wave (PAW) method was employed to explain the core-valence interactions.[6] A cutoff energy of 400 eV was chosen for the plane wave expansions. Structural optimization was conducted with an energy convergence of $1.0\times10^{-5}$ eV and a force convergence of 0.02 eV $Å^{-1}$. The Brillouin zone was sampled with the 3×3×1 K-point. Grimme's DFT-D3 methodology was used to describe the dispersion interactions.[7] The adsorption energies ($E_{ads}$) of sodium ions were consequently determined by the equation of $E_{ads} = E^{*}Na – E_{Na} – E_{Sub}$, in which E*Na is the energy after adsorbing Na on the surface, $E_{Na}$ is the energy without Na adsorption while $E_{sub}$ is the clean surface energy.

## Supplementary Figures

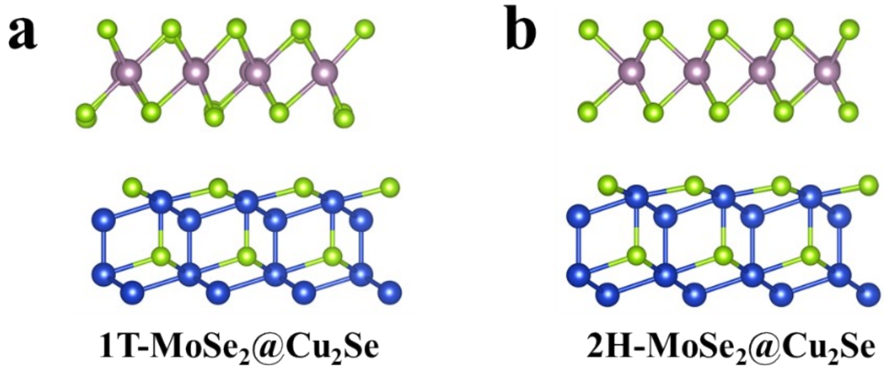


**Figure S1** Structure models of a) 1T-$MoSe_2$ and b) 2H-$MoSe_2$ after constructing heterostructures with $Cu_2Se$ for calculating the energy difference ($\Delta E = E_{1T} - E_{2H}$).

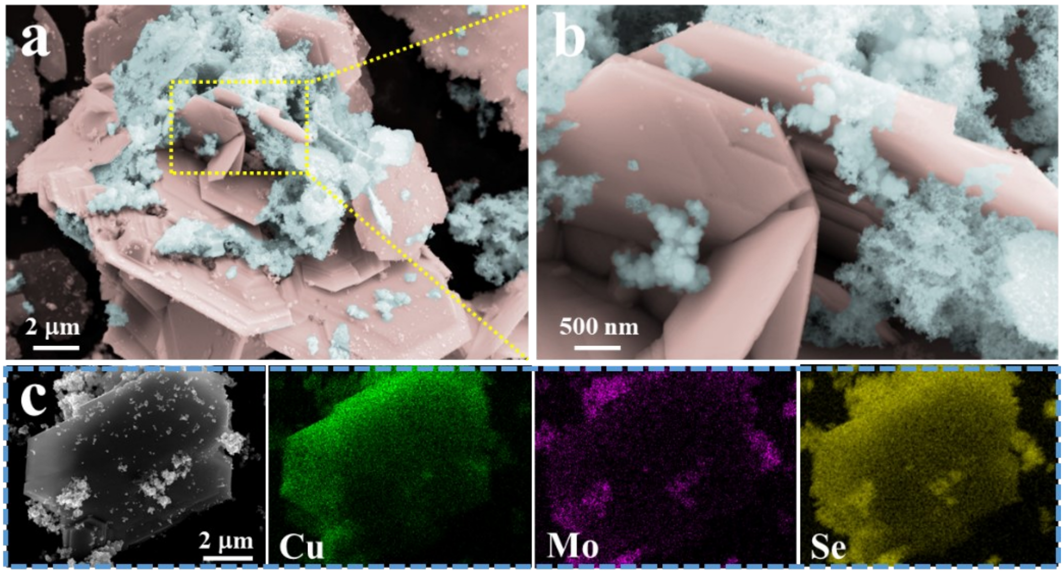


**Figure S2** Morphology of $Cu_2Se/MoSe_2$. SEM images at different magnifications (a-b) and EDS mapping images (c) demonstrating the mixing fact of $Cu_2Se$ and $MoSe_2$, which are marked by pink and light blue in the SEM images, respectively.

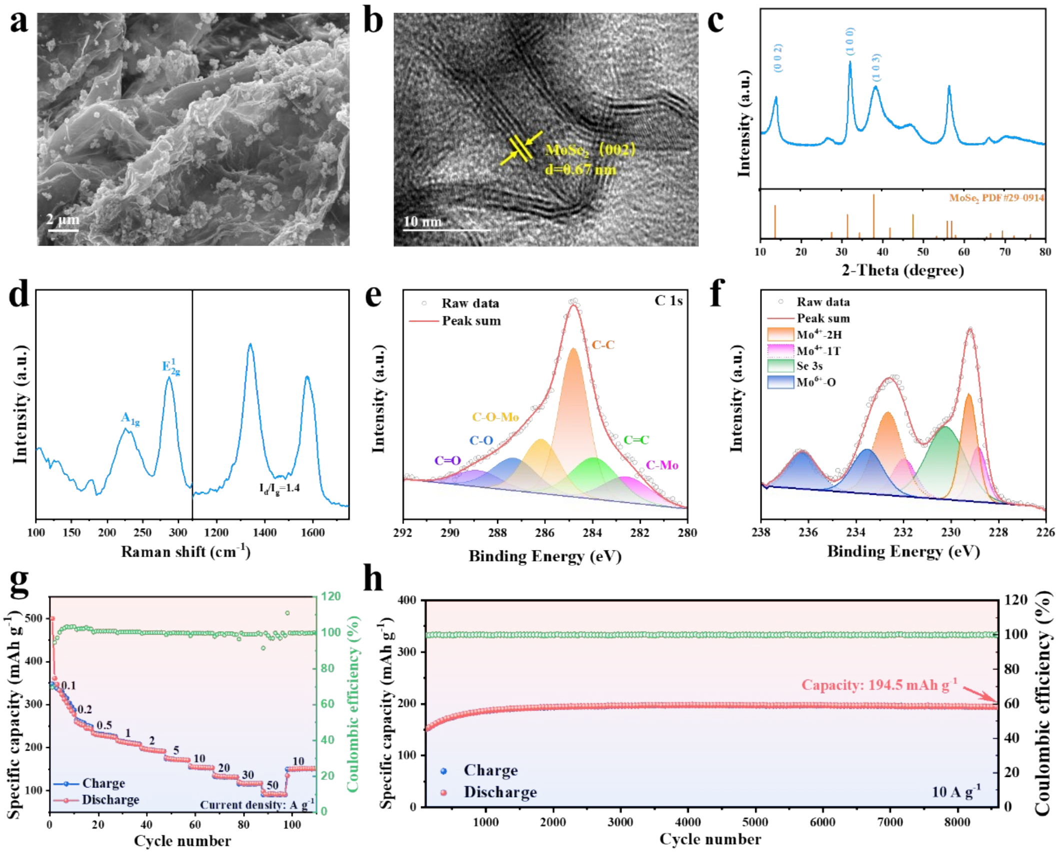


**Figure S3** Characterization and electrochemical performance of G-$MoSe_2$. SEM (a), TEM (b), XRD (c), Raman (d), Mo 3d (e), C1s (f) spectra, rate capability (g) and cycling performance (h) of G-$MoSe_2$.

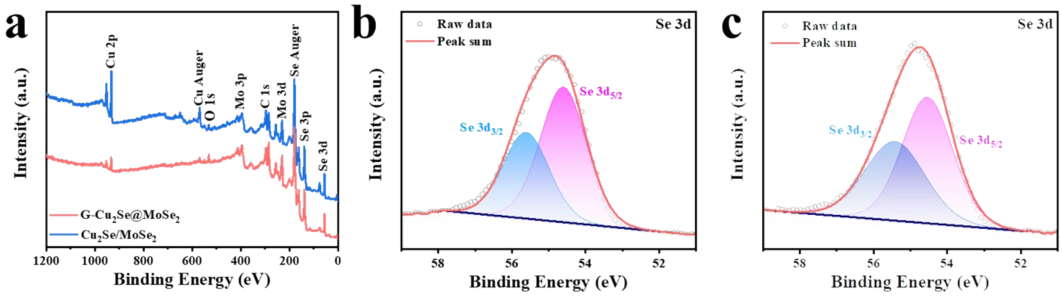


**Figure S4** (a) XPS surveys of G-$Cu_2Se$@$MoSe_2$ and $Cu_2Se/MoSe_2$; Se 3d spectra of the $Cu_2Se/MoSe_2$ (b) and G-$Cu_2Se$@$MoSe_2$ (c).

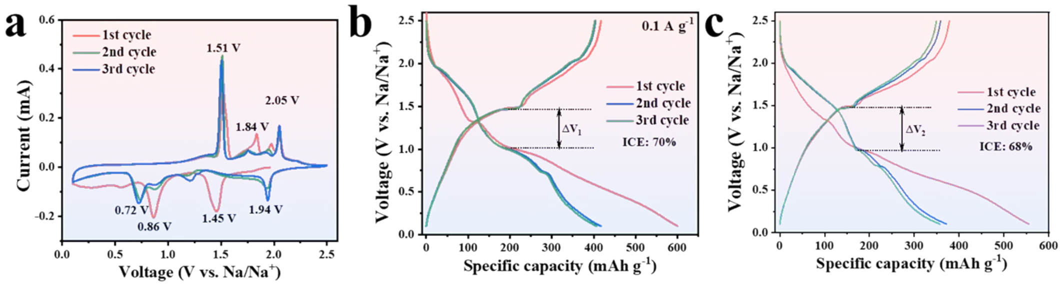


**Figure S5** (a) The first three cyclic voltammograms (CV) of $Cu_2Se/MoSe_2$ composite at a scan rate of 0.1 mV $s^{-1}$; The first three galvanostatic discharge/charge curves of (b) G-$Cu_2Se$@$MoSe_2$ and (c) $Cu_2Se/MoSe_2$ at a current density of 0.1 A $g^{-1}$.

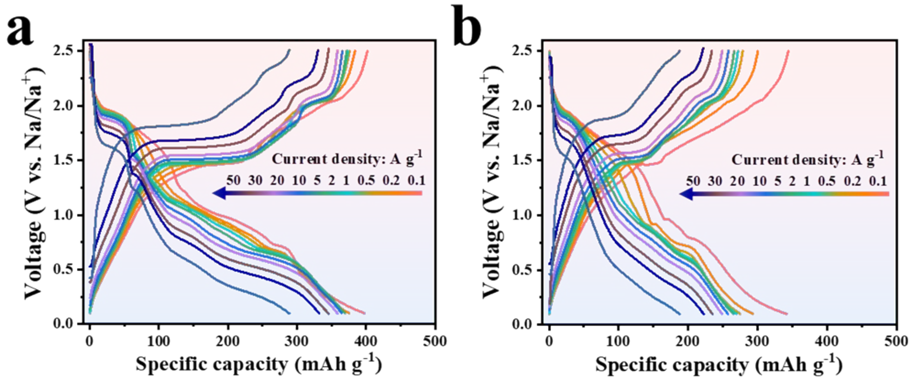


**Figure S6** Discharge/charge curves of (a) G-$Cu_2Se$@$MoSe_2$ and (b) $Cu_2Se$/$MoSe_2$composite at different current densities.

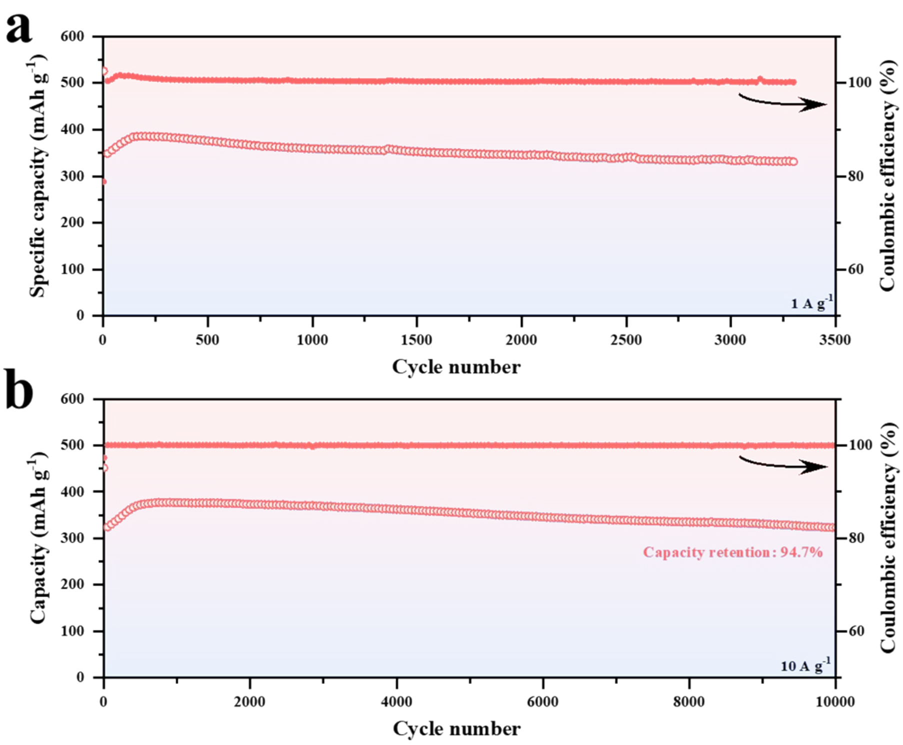


**Figure S7** Cycling performance of G-$Cu_2Se$@$MoSe_2$ at a current density of 1 A $g^{-1}$ (a) and 10 A $g^{-1}$ (b).

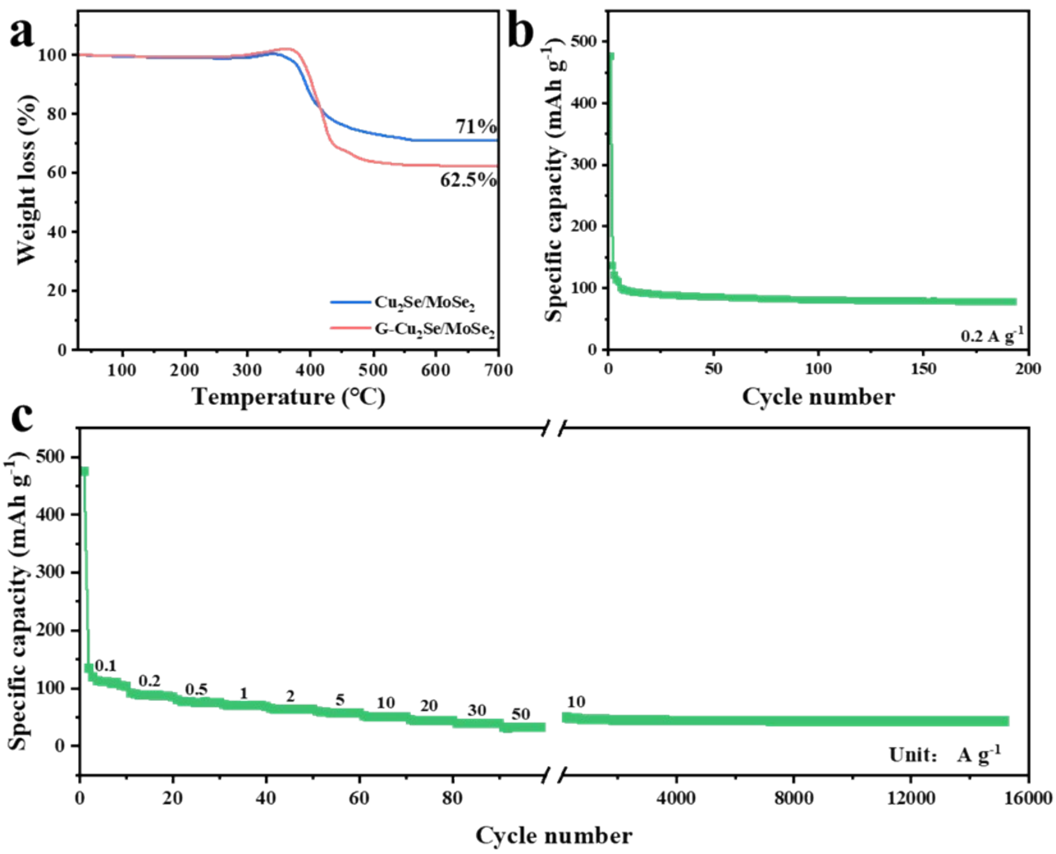


**Figure S8** (a) TG curves of $Cu_2Se@MoSe_2$ and G-$Cu_2Se@MoSe_2$ anodes; (b) Cycling performance of rGO anodes at 0.2 A $g^{-1}$; (c) Rate capability of rGO anodes and its cycling performance at 10 A $g^{-1}$.

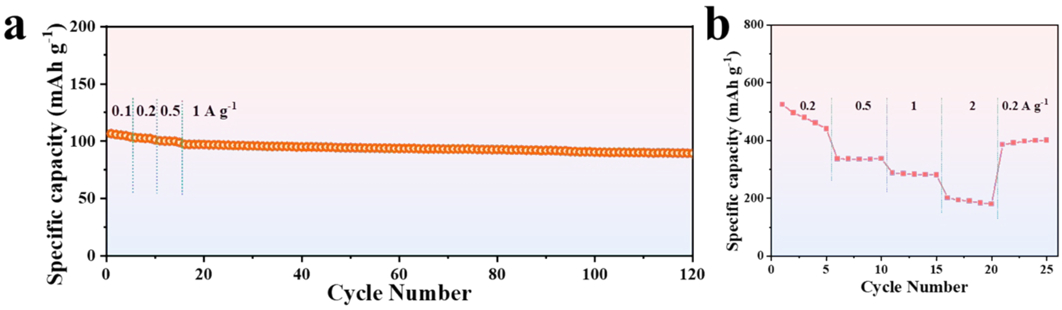


**Figure S9** (a) Rate capability and cycling performance of $Na_3V_2(PO_4)_3$ (NVP) electrode; (b) Rate capability of NVP//G-$Cu_2Se$@$MoSe_2$ full cells.

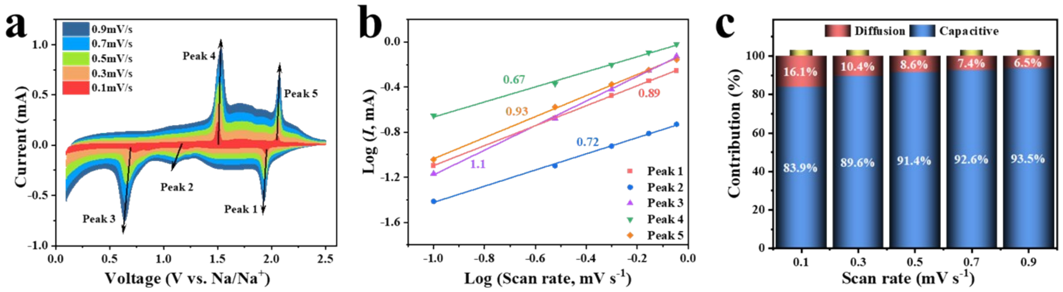


**Figure S10** (a) CV of the $Cu_2Se/MoSe_2$ electrode recorded at scan rates from 0.1 to 0.9 mV $s^{-1}$; (b) The b values of the marked peaks in (b) fitted from the logarithmic values of their peak currents and scan rates; (c) Contribution of surface-capacitive process at different scan rates of $Cu_2Se/MoSe_2$ electrode.

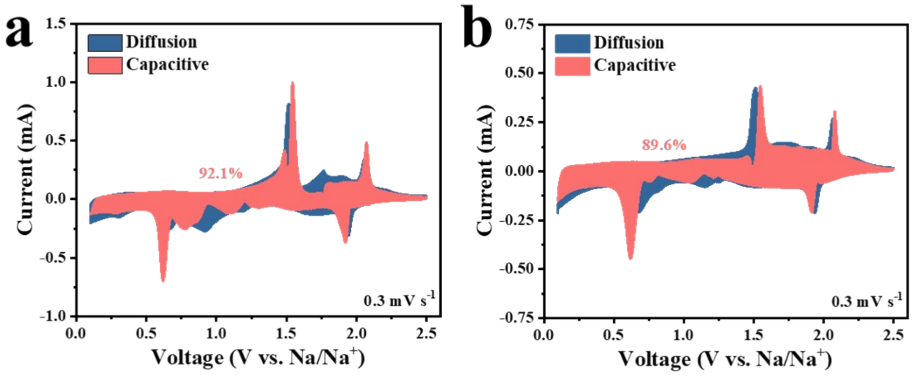


**Figure S11** CV profile of (a) G-$Cu_2Se$@$MoSe_2$ and (b) $Cu_2Se$/$MoSe_2$ showing the contribution of surface-capacitive process at 0.3 mV $s^{-1}$.

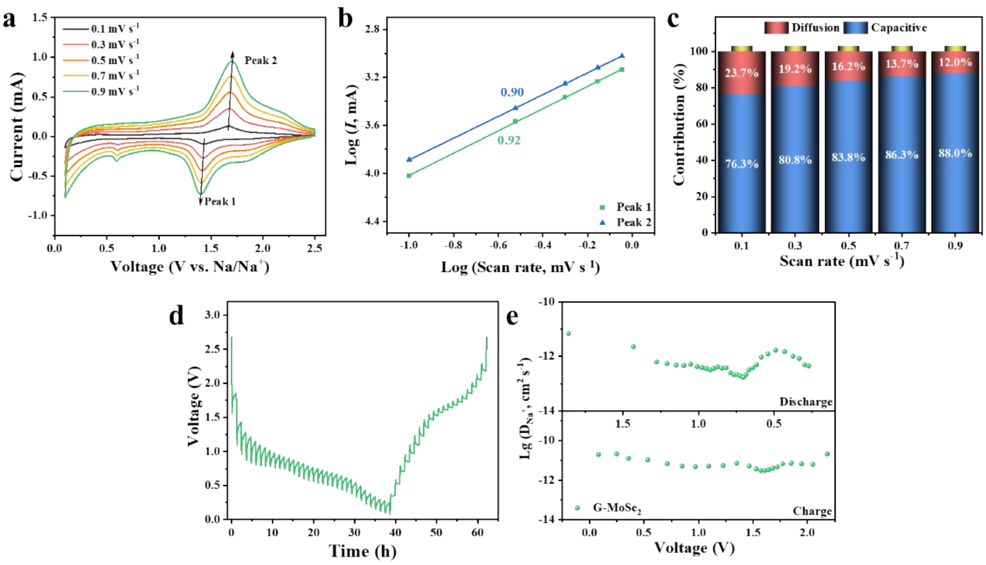


**Figure S12** (a) CV of the G-$MoSe_2$ electrode recorded at scan rates from 0.1 to 0.9 mV $s^{-1}$; (b) The b values of the marked peaks in (a) fitted from the logarithmic values of their peak currents and scan rates; (c) Contribution of surface-capacitive process at different scan rates of G-$MoSe_2$ electrode; (d) GITT curve of G-$MoSe_2$ composites; (e) Diffusion coefficient of $Na^+$ during the charge and discharge process of G-$MoSe_2$.

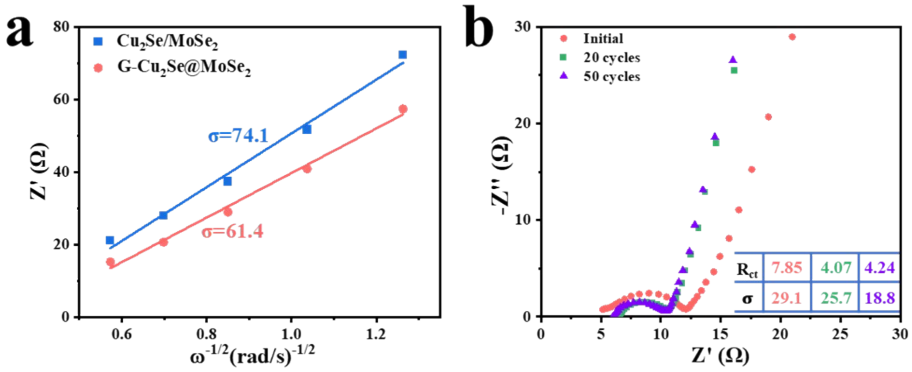


**Figure S13** (a) Linear relationship between $\omega^{-1/2}$ and Z'; (b) Nyquist plots of G-$Cu_2Se@MoSe_2$ at different charge/discharge cycles, inset is the fitted values of $R_{ct}$ and σ.

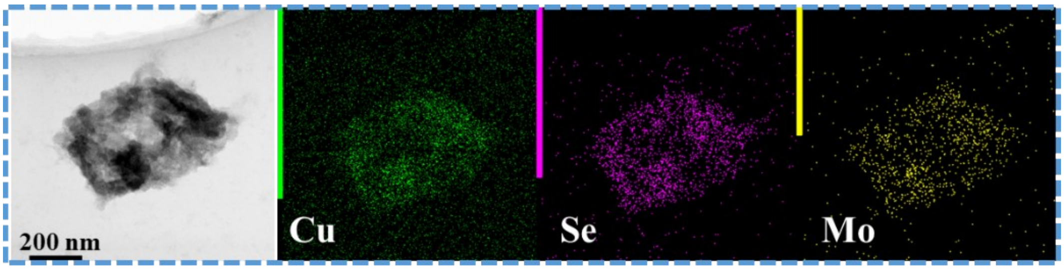


**Figure S14** EDS mapping images displaying the distribution of Cu, Mo and Se elements in cycled G-$Cu_2Se$@$MoSe_2$ composite.

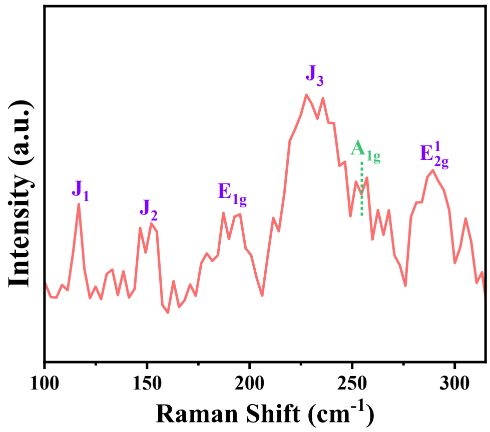


**Figure S15** Raman spectrum of cycled G-$Cu_2Se$@$MoSe_2$ anode.

**Equation S1**:

The following Equation was used to process GITT data into the diffusion coefficients of sodium ions:[8]

$$D_{Na^+} = \frac{4}{\pi\tau}\left(\frac{m_B V_m}{M_B S}\right)^2 \cdot \left(\frac{\Delta E_s}{\Delta E_t}\right)^2 = \frac{4L^2}{\pi\tau} \cdot \left(\frac{\Delta E_s}{\Delta E_t}\right)^2$$

where $m_B$ is the mass of the active materials, $V_M$ is the molar volume of the active materials, $M_B$ is the molar mass of the active materials, S is the contact area between the active materials and electrolyte, τ is the relaxation time, t is the time of duration current pulse, and $\Delta E_s$ is the potential change of steady state caused by current pulse, $\Delta E_t$ is the potential change during the constant current pulse after eliminating the iR drop. L is the diffusion length of sodium ions. For a compact electrode, L equals to the thickness of the electrode.

**Equation S2**:

The following Equation was used to calculate the $Na^+$ diffusion coefficient from the impendence data:[9]

$$D_{Na^+} = \frac{R^2T^2}{2A^2n^2F^4C^2\sigma^2}$$

in which A is the electrode area, n is the number of electronic transfers per molecule, C is the molar concentration of $Na^+$, R is the gas constant (8.314 J $mol^{-1}$ $K^{-1}$), T is the absolute temperature (298 K), F is the Faraday constant (96500 C $mol^{-1}$), σ is the Warburg factor obtained from the line slope of Z′ versus $\omega^{-1/2}$.

**References**


[1] Y. Chao, R. Jalili, Y. Ge, C. Wang, T. Zheng, K. Shu, G. G. Wallace, *Adv Funct Mater* **2017**, *27*, 1700234.

[2] G. Kresse, J. Hafner, *Phys Rev B* **1993**, *47*, 558.

[3] G. Kresse, J. Hafner, *Phys Rev B* **1994**, *49*, 14251.

[4] J. P. Perdew, K. Burke, M. Ernzerhof, *Phys Rev Lett* **1996**, *77*, 3865.

[5] G. Kresse, D. Joubert, *Phys Rev B* **1999**, *59*, 1758.

[6] P. E. Blöchl, *Phys Rev B* **1994**, *50*, 17953.

[7] S. Grimme, J. Antony, S. Ehrlich, H. Krieg, *Journal of Chemical Physics* **2010**, *132*, 154104.

[8] Y. Xu, X. Liu, H. Su, S. Jiang, J. Zhang, D. Li, *Energy & Environmental Materials* **2022**, *5*, 627–636.

[9] Y. Liang, Z. Wang, Z. Xu, S. Li, H. Luo, C. Xu, X. Cui, *Appl Surf Sci* **2024**, *651*, 159234.